Graphene-Encapsulated Nanoparticle-Based Biosensor for the Selective Detection of Cancer Biomarkers

Sung Myung, Aniruddh Solanki, Cheoljin Kim, Jaesung Park, Kwang S. Kim, and Ki-Bum Lee*

Nanomaterials such as silicon nanowires (SiNWs),[1,2] carbon nanotubes (CNTs),[3–6] and graphene,[7,8] have gained much attention for use in electrical biosensors due to their nanoscopic and electrical properties. For instance, SiNWs and CNTs can be integrated into field-effect transistors (FETs) to detect small amounts of target biomolecules with high sensitivity and selectivity by measuring electrical disturbances induced by the binding of these biomolecules to the surface of the nanostructure.[9,10] The detection of biomarker proteins with high sensitivity and selectivity is vital for the early diagnosis of many diseases including cancer and HIV. For this purpose, carbon-based nanomaterials such as CNTs and graphene have attracted significant attention for fabricating highly sensitive FET-based biosensors.[6,8,9,11–15] In particular, the use of graphene in FET-based biosensors is becoming more and more appealing not only due to its unique properties, such as higher 2D electrical conductivity, superb mechanical flexibility, large surface area, and high chemical and thermal stability, but also due to its ability to overcome the limitations of CNTs, such as variations in electrical properties of CNT-based devices and the limited surface area of CNTs.[16–24] Nevertheless, there have been only a few reports on the development of graphene FET-based biosensors,[14,25] and their potential as biosensors has not been fully explored. It is therefore critical to develop nanoscopic graphene-based biosensors that are simple in device structure, small in size, and allow label-free detection and real-time monitoring of biomarkers, all of which are essential criteria for biosensors. A key challenge in the above requirements is the achievement of both, well-organized 2D or 3D graphene structures, in microscopic and nanoscopic biosensing devices and well-defined bioconjugation chemistry on graphene.

Dr. S. Myung, A. Solanki, C. Kim, Prof. K.-B. Lee
Department of Chemistry and Chemical Biology
Rutgers, The State University of New Jersey
Piscataway, NJ 08854, USA
E-mail: kblee@rutgers.edu
Prof. K.-B. Lee
Institute for Advanced Materials
Devices and Nanotechnology (IAMDN)
Rutgers, The State University of New Jersey
Piscataway, NJ 08854, USA
J. Park, Prof. K. S. Kim
Center for Superfunctional Materials
Department of Chemistry
Pohang University of Science and Technology
Pohang, Korea

Here, we demonstrate a novel strategy for the fabrication and application of a reduced graphene oxide (rGO)[26,27] encapsulated nanoparticle (NP)-based FET biosensor for selective and sensitive detection of key biomarker proteins for breast cancer. It is important to note that we used Human Epidermal growth factor Receptor 2 (HER2) and epidermal growth factor receptor (EGFR), which are known to be over-expressed in breast cancers,[28–30] only as a proof-of-concept to demonstrate the high sensitivity and selectivity of the graphene-encapsulated NP biosensor. This biosensor could be used to detect any important cancer markers with relative ease. In the typical experiments for fabricating graphene-encapsulated NP-based biosensors, individual silicon oxide NPs (100 nm) functionalized with 3-aminopropyltriethoxysilane (APTES) were first coated with thin layers of graphene oxide (GO), which prevent aggregation and maintain high electrical conductivity (**Figure 1**). This was mainly achieved via the electrostatic interaction between the negatively charged GO (see Supporting Information, Figure S1) and the positively charged silicon oxide NPs. The GO solution (0.05 mg mL^{-1} in deionized water) was simply injected into the NP solution (5 mg mL^{-1}), wherein the negatively charged GO assembled on the positively charged NP surface until equilibrium coverage was reached.[31–33] The transmission electron microscopy (TEM) image of the GO-coated NPs clearly shows the uniform assembly and saturation density of GO on the NP surface (Figure 1a). The GO thickness on the surface of the NPs was 5 nm, as measured from high-resolution TEM (HR-TEM). As seen in the image, the NPs were connected through a film of GO that was used as an electrical carrier after its reduction to rGO. For efficient use of NP junctions as electrical channels, it was imperative to assemble the NPs with high density on the device. The scanning electron microscopy (SEM) images show well-defined, dense rGO-NP patterns uniformly covering a large area of the silicon oxide substrate (**Figure 2**a,b).

Furthermore, the modified self-assembly method (using centrifugation) allowed us to assemble NPs with high density in a short span and by using minimal amount and concentration of the NP solution. Importantly, the high surface-to-volume ratio of the GO-encapsulated NPs can generate 3D electrical surfaces that significantly enhance detection limits and enable label-free, highly reproducible detection of clinically important cancer markers.

One of the most attractive and advantageous aspects of the graphene-encapsulated NP biosensor is the ease of fabrication and measurement (Figure 2). The device was fabricated using photolithography, followed by a lift-off process, both of which are well-established.[33,34] We first generated gold electrodes on a silicon oxide substrate using photolithography and lift-off. To generate arrays of GO-NPs, we patterned the photoresist (AZ 5214) on the substrates with gold electrodes using
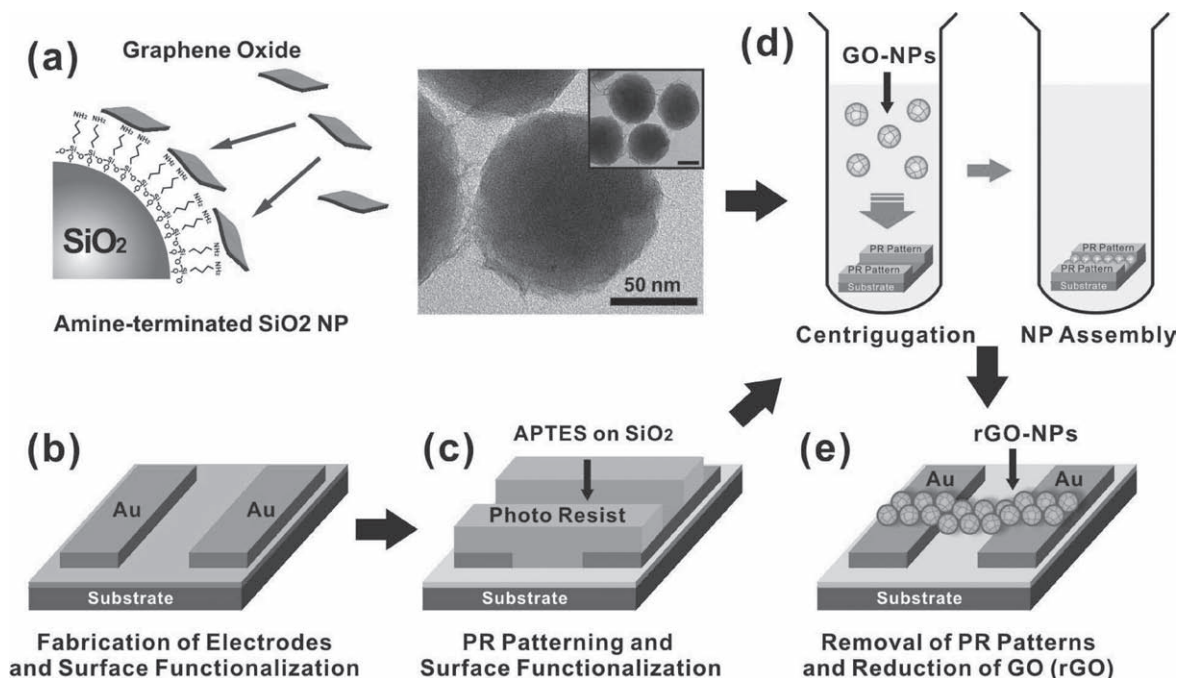
COMMUNICATION

Figure 1. Fabrication process of biomolecular sensor based on graphene-coated NPs. a) Schematic diagram of GO assembly on amine-functionalized NPs and TEM image of NPs coated with GO. b) Fabrication of a metal electrode on the oxide substrate and surface modification for the assembly of GO-NP. c) Photoresist (PR) patterns on the metal electrodes. d) GO-NP assembly in the centrifuge tube. e) Removal of PR patterns and reduction of GO coated on the NP surface.
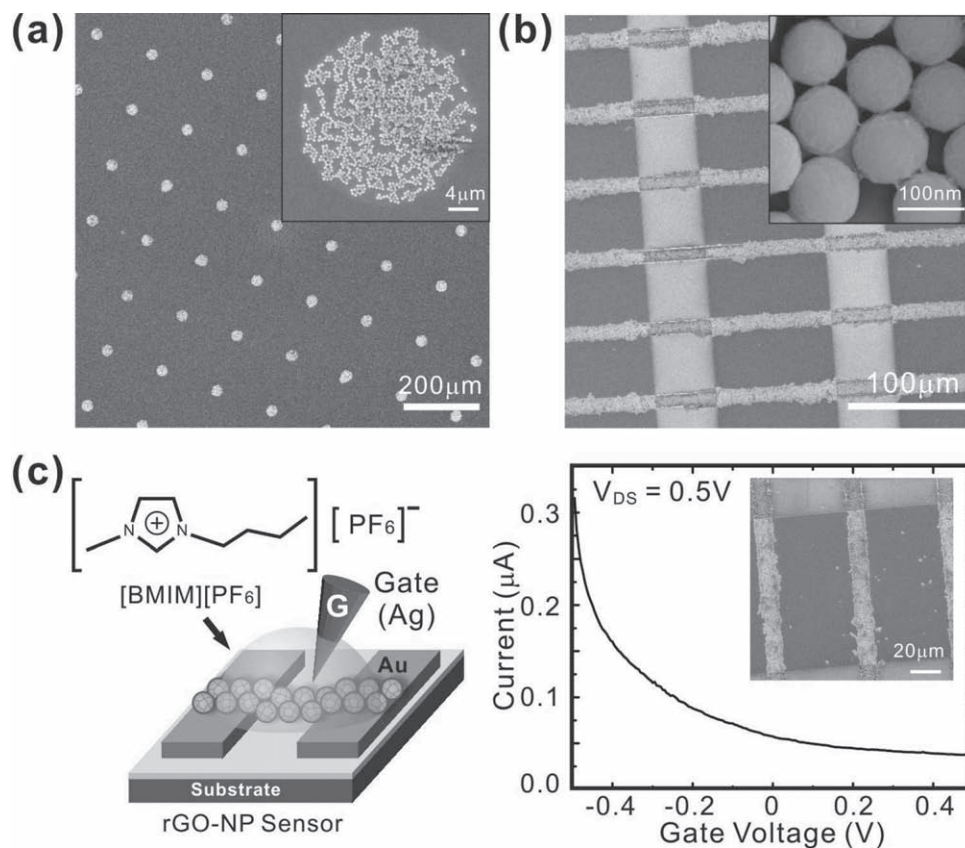

Figure 2. Reduced GO-NP patterns and the electrical property of the rGO-NP device. a) SEM images of rGO-NPs assembled on a large area. b) The SEM images of biosensors consisting of a rGO-NP array with gold electrodes. c) The schematic diagram of measuring process of the gate effect utilizing ionic liquid (left) and the gate effect of ten rGO-NP junctions with a 50 mA channel length (right).

photolithography. The exposed silicon oxide surface and gold surface were functionalized with self assembled monolayers (SAMs) of positively charged 3-aminopropyltriethoxysilane (APTES) and cysteamine, respectively. The SAM formation promoted the assembly of the negatively charged GO-NPs (through electrostatic interactions).[34,35] We then employed a relatively simple technique involving centrifugation for the uniform assembly of GO-NPs on the positively charged SAMs. In this technique, the substrate containing the patterned photoresist along with the SAMs was centrifuged in a solution of GO-NPs at 2000 rpm for 3 min in a centrifuge tube. Despite a low concentration of GO-NPs, we were able to achieve uniform films of NPs with a high density in a reproducible manner. This is in stark contrast to the standard methods used for assembling NPs on surfaces. Other methods generally rely on using larger volumes of the solution containing higher concentrations of NPs, where contact of the NPs with the surface is mainly made through infrequent Brownian motion, which eventually causes NP assembly. On the other hand, the centrifugation technique achieved uniform, very dense layers of graphene-encapsulated NPs over a large area in a short time span (Figure 2a,b). We then generated a uniform NP array by removing the patterned photoresist using acetone. The removal of photoresist did not disturb the assembly of GO-NPs. To render the insulating GO electrically conductive, we reduced the GO through an overnight exposure to hydrazine vapor. This method of fabricating the device is very powerful because it can be integrated with conventional microfabrication processes, which makes the device cost effective and relatively easy to produce on a large scale.

One of the key barriers to using graphene FET-based biosensors is to operate the device under physiological conditions (e.g., different pH and salt concentrations), in which different ionic environments affect the conductivity of graphene FET-based biosensors.[36] To study the working conditions of the graphene FET-based biosensors in aqueous solutions, we measured the gating effect of the rGO-NP-based biosensor using an ionic liquid gate (Figure 2c). A typical source–drain current versus gate potential plot was obtained in an ionic liquid, 1-butyl-3-methylimidazolium tetrafluoroborate (BmimPF$_6$) (see Supporting Information for the synthesis of BmimPF$_6$). In an ionic liquid, the high concentration of ions renders the thickness of the diffusion layer negligible, thus making it useful as a gate insulating layer. Silver (Ag) wire was used as the reference electrode for the measurements in the ionic liquid. The gating effect observed in the GO-NP devices was similar to that observed in rGO thin-film transistors that have ambipolar conduction and p-type behavior near zero gate voltage.[33,37] In the present case, the top-gate bias was swept with ≈0.05 V s^{-1} sweep speed under the source–drain bias of 0.5 V (Figure 2c).

Once the device containing the rGO-NP array was optimized for biosensing, the selective detection of HER2 and EGFR was carried out by functionalizing the rGO-NPs with monoclonal antibodies (mAbs) against HER2 or EGFR. The bioconjugation chemistry is well-established and involved three basic steps.[2,10] First, the reduced GO surface was functionalized with 4-(pyren-1-yl)butanal via π–π interactions by incubating the device in a methanol solution (1:500) of 4-(pyren-1-yl) butanal (see Supporting Information for synthesis) for 30 min (Figure 3a). Second, the aldehyde groups were coupled to the
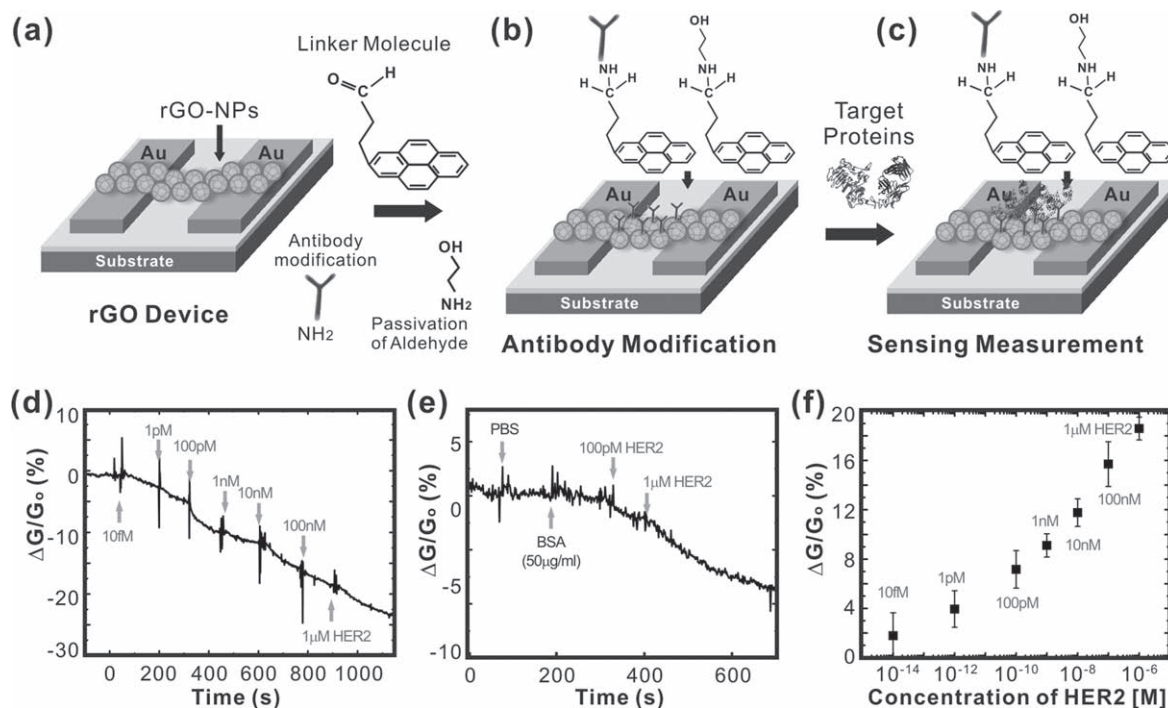

Figure 3. Real-time detection of cancer marker, HER2. a) The preparation of rGO-NP device. b) Surface functionalization of rGO for immobilizing the antibody. c) Measuring conductance of the devices when the target protein is introduced. d) The sensitivity of the biosensor (relative conductance change,%) in response to the concentration of HER2 with V_{DS} (voltage drain to source) = 1 V and V_g (gate voltage) = 0 V. e) The selectivity of the biosensor in response to PBS buffer, BSA with 50 μg mL^{-1} and HER2 (100 pM and 1 μM). f) Sensor sensitivity (relative conductance change,%) as a function of the HER2 concentration with VDS = 1 V and V_g = 0 V. All experiments were performed multiple times (sample number, n = 30) to collect statistical data (with error bars) and confirm the reproducibility and robustness of the biosensing system.

amine groups of the monoclonal HER2 or EGFR antibodies (1:50) through reductive amination in the presence of 4 mM sodium cyanoborohydride in phosphate buffered saline (PBS; pH 7.4) for 2 h (Figure 3b). Third, unreacted aldehyde groups were blocked using 100 mM ethanolamine in a similar manner to prevent non-specific interactions of proteins. Finally, we rinsed the device in a continuous flow of PBS (pH 7.4) for 10 min. We show that the surface chemistry used in the device plays a crucial role in achieving highly selective and sensitive detection of HER2 or EGFR protein (Figure 3c,d). Furthermore, due to the large surface-to-volume ratio of the rGO-NPs, the biosensors were highly efficient as compared to the thin-film-transistor-based biosensors.

The sensitivity of the rGO-NP devices, functionalized with HER2 mAbs, was determined by measuring the changes in conductance as the solution concentration of HER2 was varied from 10 fM to 1 μM (Figure 3d). In all experiments, only 1 μL of each solution was added onto the device. Representative time-dependent data show that on the addition of a 10 fM solution of HER2, no change in conductance was observed. However on increasing the concentration to 1 pM, a decrease in conductance of the p-type rGO-NP device was observed due to the binding of HER2 to the mAbs. As the concentrations of the solutions were subsequently increased, a concentration-dependent decrease in the conductance of the rGO-NP device was observed. Thus, the detection limit of the biosensor was observed to be 1 pM in a solution containing only HER2 protein, which is a significant improvement over thin-film-transistor-type sensors based on graphene.[7,14,15] The observed change in electrical conductivity can be attributed to the p-type characteristics of the rGO-NP FET-based sensors because the amine groups on the protein surface are positively charged. Binding of these positively charged target biomolecules, such as HER2 or EGFR, to the rGO surface will induce positive potential gating effects that generate reduced hole density and electrical conductance.

To test the selectivity of the graphene FET-based biosensors, we further investigated the selective detection of the device in competitive binding studies with bovine serum albumin (BSA) (Figure 3e). Time-dependent conductance measurements recorded on the rGO-NP devices functionalized with HER2 mAbs showed no change in conductance upon addition of PBS and 50 μg mL^{-1} BSA. However, upon addition of 1 μL of 100 pM solution of HER2 to the BSA solution on the device, a rapid and sharp change in conductance was observed, demonstrating the high selectivity of the device. Upon adding the 1 μM solution of HER2, the conductance further decreased rapidly and drastically. In spite of the presence of a solution with a very high concentration of BSA (50 μg mL^{-1}), the detection limit of the target protein, HER2, was 100 pM, clearly demonstrating the remarkable sensitivity and selectivity of the rGO-NP biosensor.

Figure 3f shows the sensitivity (relative conductance change) of the biosensor as a function of the HER2 concentration. The lowest HER2 concentration level that could be detected is 1 pM, which shows a decrease in conductance (3.9%). Similar to the non-linear behavior of CNT FET-based sensors,[38–40] the sensor responses increase non-linearly with the increase in the HER2 concentration from 1 pM to 1 μM, which clearly shows that the sensor response is due to the binding of HER2 to the HER2 mAbs.

In addition to HER2, we similarly investigated the sensitivity and selectivity of the device for detecting EGFR. We functionalized the device with EGFR mAbs and observed the change in conductance upon addition of EGFR solution. The trend in conductance change was similar to that observed with HER2, with the detection limit being 100 pM for EGFR and 10 nM in the presence of BSA (50 μg mL^{-1}; see Supporting Information, Figure S2). We believe the slight decrease in sensitivity for detecting EGFR (relative to HER2) might be due to the difference in binding affinities of the two mAbs to their respective proteins. However, the result demonstrates the capacity of the biosensor to detect different biomarkers in a sensitive and selective manner.

In conclusion, we have demonstrated the application of a graphene-encapsulated NP-based biosensor for highly selective and sensitive detection of cancer biomarkers by using surface chemistry principles combined with nanomaterials and micro- and nanofabrication techniques. The novel 3D structure of graphene-encapsulated NPs significantly increases the surface-to-volume ratio in FET-type biosensors, thereby improving the detection limits (1 pM for HER2 and 100 pM for EGFR) for the target cancer biomarkers. In addition, we demonstrated the highly selective nature of the biosensor as we detected low concentrations of the target cancer biomarkers in the presence of a highly concentrated BSA solution. The ease of fabrication and biocompatibility, along with excellent electrochemical and electrical properties of graphene nanocomposites, makes the graphene-encapsulated NP-based biosensor an ideal candidate for future biosensing applications in a clinical setting.

Experimental Section

Preparation of Reduced Graphene Oxide and SiO₂ NPs: GO was obtained from SP-1 graphite utilizing the modified Hummer method.[27] For the GO assembly on the surface of NPs, the GO suspension was injected into the nanoparticle solution for 10 min, and GO-NPs were separated from GO solution using a centrifuge. SiO₂ NP (100 nm) solution was purchased from Corpuscular Inc. For GO-NP assembly, the photoresist-patterned substrate was placed in the NP solution and GO-NPs were assembled on the substrate by applying centrifugal force. After the deposition of GO-NPs on the substrate, the GO on the NP surface, having the low conductance, was reduced to graphene by exposure to hydrazine vapor overnight.

Surface Molecular Pattering: 3-Aminopropyltriethoxysilane (APTES) and cysteamine molecules, used to form SAMs, and the solvents were purchased from Sigma-Aldrich. For the patterning of APTES SAM on SiO₂, the photoresist (AZ5214) was first patterned by photolithography using a short baking time (<10 min at 95 °C). The patterned substrate was placed in the APTES solution (1:500 (v:v) in anhydrous hexane) for 7 min. For the patterning of APTES on the on SiO₂ layer, the substrate with photoresist patterns was placed in an APTES solution (1:500 (v:v) in anhydrous hexane) for 10 min. The photoresist was then removed with acetone.

Metal Deposition and Measurement of Graphene Devices: For the electrode fabrication, the photoresist was first patterned on the substrate. Ti/Au (10/30 nm) was then deposited on the substrate and the remaining photoresist was then removed with acetone for the lift-off process. A Keithley-4200 semiconductor parameter analyzer was used for measurement and data collection.

Supporting Information

Supporting Information is available from the Wiley Online Library or from the author.

Materials
Views

www.MaterialsViews.com

**ADVANCED
MATERIALS**

www.advmat.de

COMMUNICATION

Acknowledgements

[1] Y. Cui, Q. Q. Wei, H. K. Park, C. M. Lieber, *Science* **2001**, *293*, 1289.

[2] F. Patolsky, G. F. Zheng, C. M. Lieber, *Nat. Protoc.* **2006**, *1*, 1711.

[3] K. Bradley, M. Briman, A. Star, G. Gruner, *Nano Lett.* **2004**, *4*, 253.

[4] R. J. Chen, H. C. Choi, S. Bangsaruntip, E. Yenilmez, X. W. Tang, Q. Wang, Y. L. Chang, H. J. Dai, *J. Am. Chem. Soc.* **2004**, *126*, 1563.

[5] A. Star, Y. Lu, K. Bradley, G. Gruner, *Nano Lett.* **2004**, *4*, 1587.

[6] X. W. Tang, S. Bansaruntip, N. Nakayama, E. Yenilmez, Y. L. Chang, Q. Wang, *Nano Lett.* **2006**, *6*, 1632.

[7] J. Lu, I. Do, L. T. Drzal, R. M. Worden, I. Lee, *ACS Nano* **2008**, *2*, 1825.

[8] S. Mao, G. H. Lu, K. H. Yu, Z. Bo, J. H. Chen, *Adv. Mater.* **2010**, *22*, 3521.

[9] A. T. Woolley, C. Guillemette, C. L. Cheung, D. E. Housman, C. M. Lieber, *Nat. Biotechnol.* **2000**, *18*, 760.

[10] G. F. Zheng, F. Patolsky, Y. Cui, W. U. Wang, C. M. Lieber, *Nat. Biotechnol.* **2005**, *23*, 1294.

[11] D. Du, Z. X. Zou, Y. S. Shin, J. Wang, H. Wu, M. H. Engelhard, J. Liu, I. A. Aksay, Y. H. Lin, *Anal. Chem.* **2010**, *82*, 2989.

[12] J. H. Jung, D. S. Cheon, F. Liu, K. B. Lee, T. S. Seo, *Angew. Chem. Int. Ed.* **2010**, *49*, 5708.

[13] C. H. Lu, H. H. Yang, C. L. Zhu, X. Chen, G. N. Chen, *Angew. Chem. Int. Ed.* **2009**, *48*, 4785.

[14] Y. Ohno, K. Maehashi, Y. Yamashiro, K. Matsumoto, *Nano Lett.* **2009**, *9*, 3318.

[15] C. S. Shan, H. F. Yang, J. F. Song, D. X. Han, A. Ivaska, L. Niu, *Anal. Chem.* **2009**, *81*, 2378.

[16] P. Avouris, *Nano Lett.* **2010**, *10*, 4285.

[17] K. S. Novoselov, A. K. Geim, S. V. Morozov, D. Jiang, Y. Zhang, S. V. Dubonos, I. V. Grigorieva, A. A. Firsov, *Science* **2004**, *306*, 666.

[18] K. S. Kim, Y. Zhao, H. Jang, S. Y. Lee, J. M. Kim, J. H. Ahn, P. Kim, J. Y. Choi, B. H. Hong, *Nature* **2009**, *457*, 706.

[19] X. S. Li, W. W. Cai, J. H. An, S. Kim, J. Nah, D. X. Yang, R. Piner, A. Velamakanni, I. Jung, E. Tutuc, S. K. Banerjee, L. Colombo, R. S. Ruoff, *Science* **2009**, *324*, 1312.

[20] K. S. Novoselov, A. K. Geim, S. V. Morozov, D. Jiang, M. I. Katsnelson, I. V. Grigorieva, S. V. Dubonos, A. A. Firsov, *Nature* **2005**, *438*, 197.

[21] Y. B. Zhang, Y. W. Tan, H. L. Stormer, P. Kim, *Nature* **2005**, *438*, 201.

[22] A. K. Geim, K. S. Novoselov, *Nat. Mater.* **2007**, *6*, 183.

[23] L. Y. Jiao, L. Zhang, X. R. Wang, G. Diankov, H. J. Dai, *Nature* **2009**, *458*, 877.

[24] X. Du, I. Skachko, A. Barker, E. Y. Andrei, *Nat. Nanotechnol.* **2008**, *3*, 491.

[25] X. C. Dong, Y. M. Shi, W. Huang, P. Chen, L. J. Li, *Adv. Mater.* **2010**, *22*, 1649.

[26] D. A. Dikin, S. Stankovich, E. J. Zimney, R. D. Piner, G. H. B. Dommett, G. Evmenenko, S. T. Nguyen, R. S. Ruoff, *Nature* **2007**, *448*, 457.

[27] G. Eda, G. Fanchini, M. Chhowalla, *Nat. Nanotechnol.* **2008**, *3*, 270.

[28] A. Citri, Y. Yarden, *Nat. Rev. Mol. Cell Biol.* **2006**, *7*, 505.

[29] N. E. Hynes, H. A. Lane, *Nat. Rev. Cancer* **2005**, *5*, 341.

[30] Y. Yarden, M. X. Sliwkowski, *Nat. Rev. Mol. Cell Biol.* **2001**, *2*, 127.

[31] I. Jung, D. A. Dikin, R. D. Piner, R. S. Ruoff, *Nano Lett.* **2008**, *8*, 4283.

[32] T. Kobayashi, N. Kimura, J. B. Chi, S. Hirata, D. Hobara, *Small* **2010**, *6*, 1210.

[33] S. Myung, J. Park, H. Lee, K. S. Kim, S. Hong, *Adv. Mater.* **2010**, *22*, 2045.

[34] S. Myung, M. Lee, G. T. Kim, J. S. Ha, S. Hong, *Adv. Mater.* **2005**, *17*, 2361.

[35] M. Lee, J. Im, B. Y. Lee, S. Myung, J. Kang, L. Huang, Y. K. Kwon, S. Hong, *Nat. Nanotechnol.* **2006**, *1*, 66.

[36] W. R. Yang, K. R. Ratinac, S. P. Ringer, P. Thordarson, J. J. Gooding, F. Braet, *Angew. Chem. Int. Ed.* **2010**, *49*, 2114.

[37] F. Chen, Q. Qing, J. L. Xia, J. H. Li, N. J. Tao, *J. Am. Chem. Soc.* **2009**, *131*, 9908.

[38] A. Star, J. C. P. Gabriel, K. Bradley, G. Gruner, *Nano Lett.* **2003**, *3*, 459.

[39] M. Abe, K. Murata, A. Kojima, Y. Ifuku, M. Shimizu, T. Ataka, K. Matsumoto, *J. Phys. Chem. C* **2007**, *111*, 8667.

[40] B. L. Allen, P. D. Kichambare, A. Star, *Adv. Mater.* **2007**, *19*, 1439.